FEATURE ARTICLE

Terahertz Studies of Collision-Broadened Rotational Lines

H. Harde

Universität der Bundeswehr Hamburg, Holstenhofweg 85, 22043 Hamburg, Germany

R. A. Cheville and D. Grischkowsky*

School of Electrical and Computer Engineering and Center for Laser and Photonics Research, Oklahoma State University, Stillwater, Oklahoma 74078

Received: September 26, 1996; In Final Form: March 7, 1997[⊗]

Via terahertz (THz) coherent transients and THz time-domain spectroscopy, we have measured the far-wing absorption line profile of the ensembles of collision-broadened ground state rotational lines of methyl bromide, methyl chloride, and methyl fluoride vapors out to more than 200 line widths from resonance, corresponding to frequency offsets as much as 5 times the resonant frequency. On these far wings the measured absorption is approximately an order of magnitude less than that predicted by the van Vleck−Weisskopf theory. Our observations show that as the offset frequency is increased, a transition occurs from the regime of the van Vleck−Weisskopf theory to the regime of the Lorentz theory. These measurements are fit to a new molecular response theory which explicitly includes the molecular orientation time during a collision. Due to the broad bandwidth of the THz pulses, we demonstrate the validity of this molecular response theory for the far-wing absorption of methyl fluoride, chloride, and bromide. The excellent theoretical fit to our measurements encompassing the frequency range over which this transition occurs indicates a molecular response time on the order of 200 fs. These measurements also permit determination of the line-width dependence on the rotational quantum number *J*.

I. Introduction

Important information on the collision behavior and intermolecular forces is obtained through the width and shape of broadened spectral lines from optical to microwave frequencies.[1−3] The near-resonance part of the line shape is mainly determined by the collision frequency or time between collisions. However, the far wings of the resonance lines are strongly influenced by the interaction forces between molecules which occur during the collision itself.

The analysis of most spectroscopic data is performed using two line shapes based on two different orientational distributions after a collision. The line shape of Lorentz[4] assumes that after a collision the molecules are oriented randomly with respect to the applied electromagnetic field. This assumption prevents the Lorentz theory from reducing to that of Debye in the zero-frequency resonant case. This discrepancy was removed by van Vleck and Weisskopf, who developed a line-shape theory based on the assumption that after a collision the molecules are oriented along the direction of the applied field with a Boltzmann distribution. This assumption requires the duration of the collision be short compared to the period of oscillation of the field. For the higher frequencies of optical and infrared transitions, the Lorentzian line shape[4] provides excellent agreement with experiment, particularly for the central region of the line. As the frequencies are reduced to those of the microwave or far-infrared region, and under conditions when a line width becomes comparable with the transition frequency, the absorption profile of a spectral line is better represented by the van Vleck−Weisskopf line shape.[5−8]

Studies of collisionally broadened line shapes have impact beyond understanding molecular interactions during collisions for a wide variety of problems of practical interest. These include applications for electromagnetic propagation and remote sensing in the atmosphere where the broad continuum absorption from water vapor leads to higher than expected loss.[9] This continuum absorption is not yet completely understood; both anomalous far-wing absorption and water dimers or larger clusters have been proposed to explain the continuum absorption.[10] Determination of accurate line shapes is also important for analysis of astronomical data, where spectroscopy is often the only practical method of obtaining information about the celestial bodies of interest. The wide range of conditions of these observations, from the extremely low densities of interstellar space to high pressures and temperatures of planetary atmospheres, presents both theoretical and experimental challenges.

Using the techniques of THz coherent transients and THz time-domain spectroscopy (THz-TDS), we have extended such line-shape investigations to THz frequencies with the goal of gaining some insight into the actual collision process itself. Our investigations are now giving information on the duration of the strong state-changing collisional interaction since we are able to sensitively investigate the far wings of rotational lines.

To study the spectral line shapes of absorption and dispersion, we measure coherent transient effects in the time domain,[11,12] which result from the interaction of a short pulse of THz electromagnetic radiation with the resonant systems.[13−16] These experiments were based on exciting molecular vapors with freely propagating subpicosecond pulses of THz radiation and detecting the free induction decay (FID) reradiated by the vapors. The

[⊗] Abstract published in *Advance ACS Abstracts,* May 1, 1997.

S1089-5639(96)02974-X CCC: $14.00

propagation of a THz pulse through a molecular vapor simultaneously excites a manifold of rotational transitions, thereby causing the molecules to radiate a FID signal.[13−16] Since the molecules studied in this investigation (methyl bromide, methyl chloride, and methyl fluoride) are distinguished by absorption lines with an almost constant frequency spacing, after the initial THz excitation a periodic rephasing and dephasing of the entire ensemble of excited rotational transitions (in the case of methyl bromide more than 130 lines) occurs during the free induction decay. This rephasing process is manifest as a train of subpicosecond THz pulses with a repetition rate equal to the frequency separation between adjacent lines. These periodic pulses are termed "THz commensurate echoes".[13] For a similar phenomenon of infrared pulses emitted after excitation see refs 17−20. By taking a numerical Fourier transform of the measured time-resolved electric field pulse train including the commensurate echoes, a direct determination of the frequency-dependent absorption and dispersion of the sample can be obtained over the entire bandwidth of the THz pulse, extending from low frequencies up to 5 THz.

The measured time-resolved THz echoes carry almost complete information about the molecular system. We obtain the molecular constants and from the echo decay the coherence relaxation time T_2, determined only by collisional dephasing, since Doppler and lifetime broadening are completely negligible in this frequency range. We have measured, with a time resolution of better than 100 fs, trains of echoes extending to beyond 300 ps. These measurements are compared with theoretical simulations using linear dispersion theory. In our analysis the linear response of the molecules to the propagating THz pulses was obtained in the frequency domain, and from the resulting spectral response the time-domain behavior was determined. A fit of the calculated pulse structure to the measurements determined T_2 over more than 2 orders of magnitude of vapor pressure and up to pressures at which the absorption lines would be completely overlapping in the frequency domain. Owing to the high signal-to-noise ratio and the exceptional time resolution, the line shape and the strong variation of the pressure broadened line widths over the rotational spectrum were obtained.

In the THz experiments reported here, we have measured the absorption line shapes in the ground state rotational bands of methyl bromide, methyl chloride, and methyl fluoride vapors from resonance to frequency offsets as much as 5 times the resonant frequency and to as much as 200 line widths away. Our measurements are well fit using a van Vleck−Weisskopf line shape for an individual transition out to frequency offsets of the order of 1 THz. Further increasing the offset leads to a much reduced absorption compared to that of the van Vleck−Weisskopf line shape.[16] In fact, we find that at higher frequency offsets the measured absorption is almost an order of magnitude less than that given by the van Vleck−Weisskopf line shape.

In our initial investigations,[16] we were able to obtain an excellent fit to our early methyl chloride measurements by using the van Vleck−Weisskopf theory for relatively low frequencies and with a simple empirical weighting function switching to the Lorentz theory for the high-frequency part. The frequency range of the transition between the two theories was interpreted to indicate the duration of the molecular collision. Our initial empirical theory[16] provided only a first-order approximation to a more inclusive theory which would handle the transition from van Vleck−Weisskopf to Lorentzian theory.

Such a molecular response theory has been developed and is presented for the first time in this paper. In brief, the response of an ensemble of harmonic oscillators to an oscillating electric field is obtained, where the polarization of the oscillators over the collision time is considered. Our approach provides the first dielectric response function describing such a system, where the collision duration occurs naturally in the theory together with the mean time between collisions. The molecular response theory reduces to that of the van Vleck−Weisskopf or Lorentz theories in the appropriate limits. The theoretical model as well as our measurements interprets the previously introduced collision parameter[16] τ_c as the response time of molecules orienting to an external field in the presence of molecular collisions.

This theory is developed from the framework of van Vleck−Weisskopf and Lorentz, who considered macroscopic polarizations of ensembles with given statistical distributions after a collision. The fact that only macroscopic polarizations are considered is in contrast to many recent line-shape theories,[21,22] developed from the seminal work of Anderson[8] and Tsao and Curnutte.[23] All these theories are derived from a microscopic point of view and consider the interaction of colliding species through their trajectories and intermolecular potentials. These theories also predict line shapes different than those of the van Vleck−Weisskopf and Lorentz theories, with the details strongly dependent on the intermolecular potential and trajectory. Variations of the line shape for collisions of finite duration, similar to our assumption of τ_c, have been calculated using the microscopic type of theory.[24]

In contrast to the seminal paper of van Vleck and Weisskopf,[5] where the key parameter is the collision duration compared to the angular frequency ω of the applied radiation, we have now shown via molecular response theory that the significant parameter is not $\omega\tau_c$, but has to be replaced by the two parameters $(\omega - \omega_{JK})\tau_c$ and $(\omega + \omega_{JK})\tau_c$. This situation indicates that the detuning from the resonance frequency ω_{JK} is important rather than the absolute frequency, as is expected from harmonic oscillator theory. In agreement with this condition, our observations are explained by the following picture. At lower frequency offsets the measurements satisfy the (extended) van Vleck−Weisskopf condition that the collision duration is short compared to the period of oscillation of the applied field (now the periods of the sum and difference frequencies). However, as the frequency offset is further increased the above condition is violated, and the original approximation of Lorentz is approached as a limiting case, where it is assumed that the molecules are randomly oriented with respect to the applied field after a collision.

The remainder of this paper is organized as follows: section II introduces the experimental technique of terahertz time-domain spectroscopy (THz-TDS) used for measurements on the methyl halides with an emphasis on the capabilities and limitations for THz (far-infrared) spectroscopy. Section III presents THz-TDS measurements in methyl fluoride, methyl chloride, and methyl bromide. Section IV develops the molecular response line-shape theory that ties together the van Vleck−Weisskopf and Lorentz theories through the inclusion of the molecular orientation time. The fifth section of the paper is devoted to detailed comparisons between measurements and theory over 2 orders of magnitude pressure range and the calculated response of the methyl halides for the various line shapes developed in section IV. These measurements clearly show the transition between the van Vleck−Weisskopf and Lorentz line shapes that is well explained by our molecular response line-shape theory. In the final section we summarize the work and discuss several possible applications of THz time-domain spectroscopy to problems in physical chemistry.

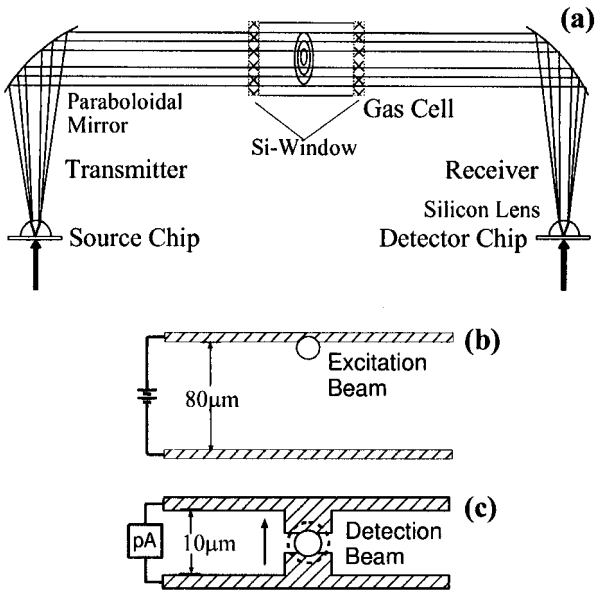

Figure 1. (a) THz collimating and focusing optics together with a vapor cell. (b) Optoelectronic configuration used to generate the freely propagating pulses of THz radiation. (c) Receiving antenna geometry.

II. Experimental Setup

For our investigations we used the powerful technique of THz-TDS.[13−16,25−29] With this technique two electromagnetic pulse shapes are measured, the input (reference) pulse and the propagated pulse, which has changed shape due to its passage through the sample under study. Consequently, via Fourier analyses of the input and propagated pulses, the frequency-dependent absorption and dispersion of the sample can be obtained. Owing to the broad bandwidth of the THz pulses, a spectral range extending from less than 100 GHz up to more than 5 THz can be investigated.

The experimental system[13−16,25−29] used for THz coherent transients and THz-TDS is shown in Figure 1a. THz pulses are optoelectronically generated by the ultrashort laser pulses incident on the optoelectronic source chip. The generated THz beam is collimated by a silicon lens, which is attached to the back of the source chip and whose front surface is located at the focus of the paraboloidal mirror. The collimated THz beam propagates and diffracts to the paraboloidal mirror, where the THz radiation is recollimated into a highly directional beam with beam diameters proportional to the wavelength and with a frequency-independent divergence of typically 25 mrad. This combination of the paraboloidal mirror, silicon lens, and the optoelectronic THz source chip comprises the THz transmitter. A second identical paraboloidal mirror and silicon lens combination on the receiving end focuses the THz beam on the detector and comprise the THz receiver.

The high-performance optoelectronic source chip[30] is shown in Figure 1b. The simple coplanar transmission line structure consists of two 10 μm wide metal lines separated by 80 μm, fabricated on high-resistivity GaAs, and dc biased at 80−100 V. Irradiating the metal−semiconductor interface (edge) of the positively biased line with focused ultrafast laser pulses produces synchronous bursts of THz radiation. This occurs because each laser pulse creates a large number of photocarriers in a region of extremely high (trap enhanced) electric field.[31] The consequent acceleration of the carriers generates the burst of radiation. Two laser systems were used in collecting the data presented here. For earlier data (mainly methyl fluoride and chloride at low pressures) the excitation source was a colliding-pulse mode-locked (CPM) dye laser. This laser produces 623 nm, 60 fs excitation pulses at a 100 MHz repetition rate in a beam with an average power of 5 mW at the 10 μm diameter excitation spot. The remainder of the data were collected using a mode-locked Ti:sapphire laser generating 70 fs excitation pulses at 820 nm.

The THz receiver chip has an antenna geometry shown in Figure 1c. The antenna is fabricated on an ion-implanted silicon-on-sapphire (SOS) wafer. The 20 μm wide antenna structure is located in the middle of a 20 mm long coplanar transmission line consisting of two parallel 10 μm wide, 1 μm thick, 5 Ω/mm aluminum lines. For data at the lower frequency ranges the separation of the coplanar strip line structure was 30 μm. Higher frequency response was obtained using a shorter dipole antenna with a 10 μm strip-line spacing. The electric field of the focused incoming THz radiation induces a transient bias voltage across the 5 μm gap between the two arms of the receiving antenna, which are directly connected to a low-noise current amplifier. The amplitude and time dependence of this transient voltage is obtained by measuring the collected charge (average current) versus the time delay (determined by a computer-controlled stepping motor with interferometric precision) between the THz pulses and the delayed laser pulses in the 5−10 mW detection beam. These laser pulses synchronously gate the receiver, by driving the photoconductive switch defined by the 5 μm antenna gap. Simply speaking, the switch is closed by the photocarriers created by the femtosecond laser pulse; the switch then reopens in approximately 600 fs due to the short carrier lifetime in ion-implanted SOS.

The THz receiver has been shown capable of detecting pulses with a time resolution faster than 100 fs corresponding to a frequency range from 0.2 THz to more than 4 THz (1 THz = 33.3 cm^{-1} = 4.1 meV) coming at a 100 MHz repetition rate with a signal-to-noise ratio of approximately 10 000:1 (see refs 29 and 30). Based on previous calculations[29] and direct measurements, the average THz power incident on the sample is 10 nW. For a signal-to-noise ratio of unity and a bandwidth of 1.6 Hz, the demonstrated detection limit is 10^{-16} W. Because the generation and detection of the THz (far-infrared) radiation are coherent, the THz receiver is intrinsically 1000 times more sensitive than an incoherent, liquid helium cooled bolometer.[32] In addition, because of the gated and coherent detection, the thermal background, which plagues traditional measurements in this THz (far-infrared) frequency range, is observationally absent.

Three different vapor cells, located as shown in Figure 1a, were used. Early results with methyl fluoride and methyl chloride were obtained using a 22.5 cm path length cell constructed of stainless steel with a clear aperture of 4 cm. The windows consisted of 2 cm thick, 5 cm diameter, high-resistivity (10 kΩ cm) silicon. Silicon is an optimal window material, due to its almost complete transparency and lack of dispersion in the THz frequency range.[28] To maximize sensitivity to far-wing absorption in spectrally dense gases, a 38.2 cm path length cell constructed of brass was used. This cell was also equipped with 2 cm thick high-resistivity silicon windows. Measurements optimizing sensitivity near the center of the rotational line manifold on spectrally dense samples were made in a cell with a path length of 2.27 cm constructed of aluminum. This cell was equipped with 1 cm thick high-resistivity silicon windows. The entire THz system is located in an airtight enclosure to mitigate the effects of water vapor on the THz beams.[26,27]

The cells were filled with methyl fluoride, methyl chloride, and methyl bromide using a gas manifold with three separate

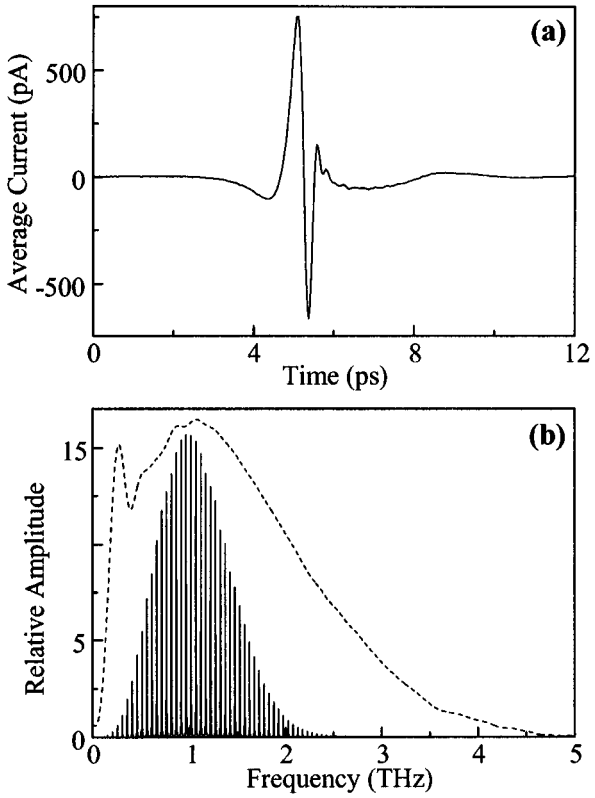

Figure 2. (a) Measured THz reference pulse (transmitted THz pulse through an empty vapor cell). (b) Relative amplitude spectrum of the reference pulse compared with the calculated absorption spectrum of methyl fluoride vapor for the ground state rotational band at a pressure of 10 hPa.

capacitance manometer gauges (MKS Baratron) to measure pressures in the range 0−100, 0−1000, and 0−5000 Torr. The cell was evacuated to <1 mTorr using a roughing pump between each series of measurements. Upon filling the cell, adsorption at the cell wall caused slight pressure drops over time. A metering valve was used to control cell pressures during data acquisition to ±2.5 Torr. The gas was allowed time to come into thermal equilibrium with room temperature after each fill, and a thermocouple sensor accurate within 0.1 K monitored the cell temperature.

The most serious limitation to the accuracy of our measurements involves the relatively long-term changes in the laser pulses and the consequent changes in the input THz pulses. During an experiment, we first measure the reference THz pulse (cell under vacuum), then measure the THz pulse transmitted through the sample, and finally remeasure the reference pulse with the sample removed. This sequence is repeated several times to obtain good statistics. Typically, the amplitude spectral ratio of subsequent reference pulses varies by ±3% over the THz frequency spectrum. In the same manner, the relative phase of subsequent reference pulses varies by ±0.03 rad over the same spectrum.

A measured transmitted reference THz pulse is displayed in Figure 2a, where the time duration from maximum to minimum is seen to be 0.45 ps. The system noise level is 0.5 pA. The corresponding amplitude spectrum, obtained by a numerical Fourier transform of Figure 2a, shows a bandwidth extending well beyond 4 THz in Figure 2b, in direct comparison with the calculated room-temperature methyl fluoride rotational band. Almost all of the polar molecules have their rotational absorption lines within this frequency range and therefore can be investigated with THz pulses.

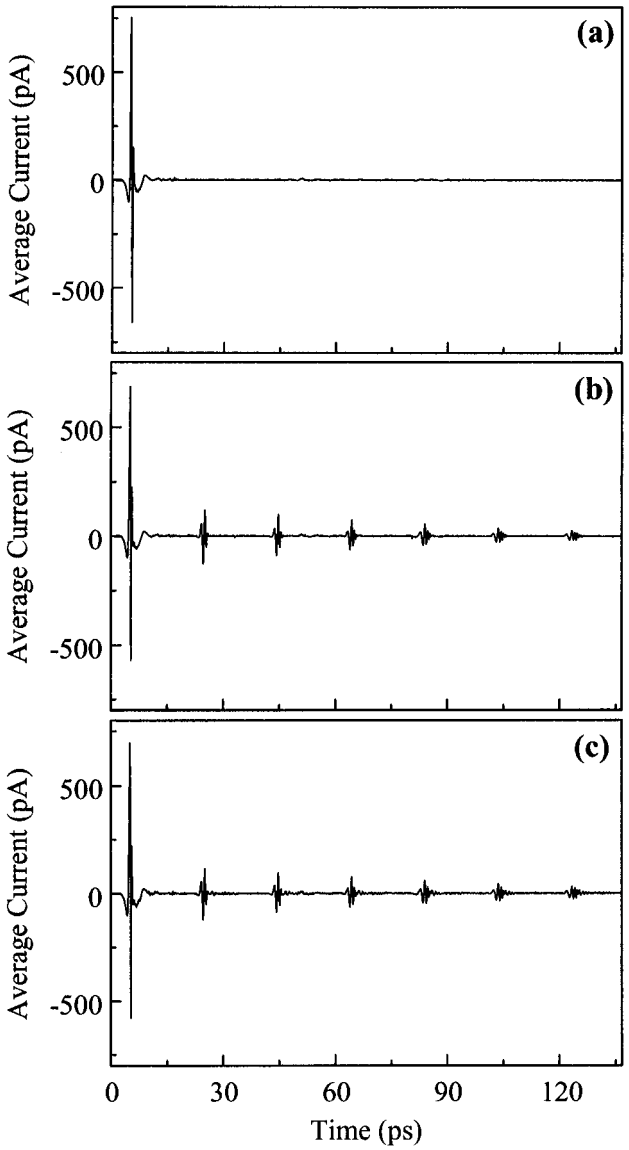

Figure 3. (a) THz reference pulse measured without vapor in the cell. (b) Measured transmitted THz pulse through 22.5 cm of 10 hPa of methyl fluoride vapor. (c) Calculated transmitted THz pulse.

III. Measurements

A THz pulse propagating through a methyl halide vapor will be reshaped due to the absorption and dispersion of the vapor. These changes can be dramatic and are quantified by comparing the transmitted pulse to the reference pulse, as demonstrated by the measurements presented in Figure 3. The reference pulse shown in Figure 3a is the same pulse shown in Figure 2a, but here on an extended time scale. This pulse illustrates the rapid response of the system, the clean base line, and the excellent signal-to-noise ratio. When 10 hPa (7.5 Torr) of methyl fluoride vapor is added to the cell, the transmitted pulse changes to that shown in Figure 3b. The reshaped and attenuated excitation pulse is followed by a series of coherent transients,[13−16,26,27] which rapidly decay because of the collisional broadening. The relative amplitude of the first transient is one-fifth that of the excitation pulse, and well-defined subpicosecond coherent transients appear every 20 ps. As shown in Figure 2b, within the broad spectral range covered by the THz pulses the methyl fluoride molecule has a manifold of pure rotational absorption lines which are simultaneously excited by the THz pulse. At frequencies higher than 2.5 THz the absorption is almost exclusively determined by the far wings of the rotational lines.

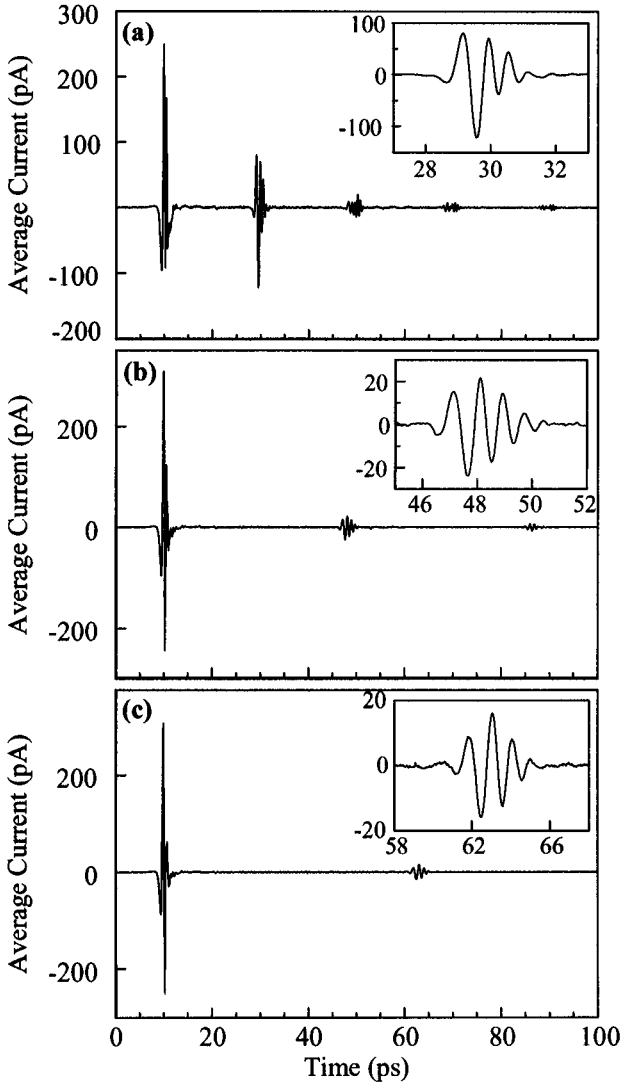

Figure 4. Measured transmitted THz pulses through 2.27 cm of 666 hPa of methyl halide vapors. The insets show the first commensurate echoes on an expanded scale: (a) methyl fluoride, (b) methyl chloride, (c) methyl bromide.

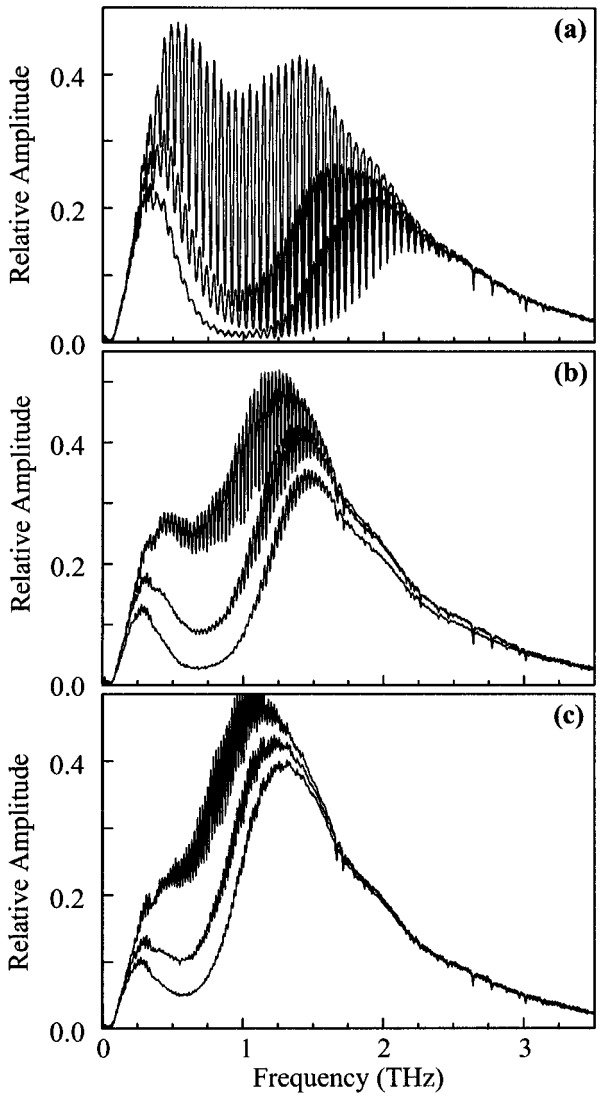

Figure 5. Measured THz-TDS absorption spectra from the THz pulses transmitted through 2.27 cm of 666, 1333, and 2000 hPa pressures: (a) methyl fluoride, (b) methyl chloride, (c) methyl bromide.

All information contained in the frequency-dependent amplitude and phase spectra of the molecular vapor is contained in the free induction decay signal measured directly in the time domain. The 20 ps temporal spacing between the coherent transients corresponds to the inverse frequency spacing (approximately 50 GHz) of the rotational lines of methyl fluoride, and the decay of the commensurate echo amplitude provides information on the collisional dephasing time T_2. This can be seen more dramatically in Figure 4, where the response of methyl fluoride, chloride, and bromide are all measured in the 2.27 cm cell at a pressure of 666 hPa. The first commensurate echo is shown on an expanded time scale in the insets. As expected, the spacing between the echoes increases with increasing mass of the molecule, corresponding to the closer rotational line spacing in the frequency domain. The rotational line manifolds can be seen in the corresponding absorption spectra shown in Figure 5, obtained by a numerical Fourier transform from the time-domain measurements. The manifold of rotational states populated at room temperature falls well within the bandwidth of the THz pulses for all three vapor samples. As the pressure increases, the rotational band which is clearly visible at 666 hPa becomes nearly a smooth curve at 2000 hPa when the lines already strongly overlap. The spectra also indicate the variation of the line width with rotational quantum number J which is observable as a lower resolution between the broader lines at the low-frequency side and the stronger modulation between narrower lines at the high-frequency side of the absorption band. The isolated absorption lines appearing at high frequencies are due to small impurities of water vapor in the investigated samples.

More in depth information may be obtained by looking at selected echo pulse structures on a magnified time scale. Such measurements are only possible due to the high performance of the optoelectronic THz system. Figure 6 is an expanded view of Figure 3 showing the excitation pulse, the first and the sixth echo emitted by the sample 20 and 120 ps after the excitation pulse, respectively. These echoes show significant reshaping with increasing echo number due to several effects. One contribution is that the methyl halide molecules show small deviations from the rigid-rotator model. As centrifugal forces increase the moment of inertia of the rotating molecule, the frequency spacing between adjacent rotational lines is no longer constant but decreases slightly with increasing rotational quantum number J. Each rotational line further consists of a series of transitions associated with the quantum number K, representing the projection of the angular momentum on the molecular symmetry axis. Due to the centrifugal stretching perpendicular to this axis, the degeneracy of the K transitions

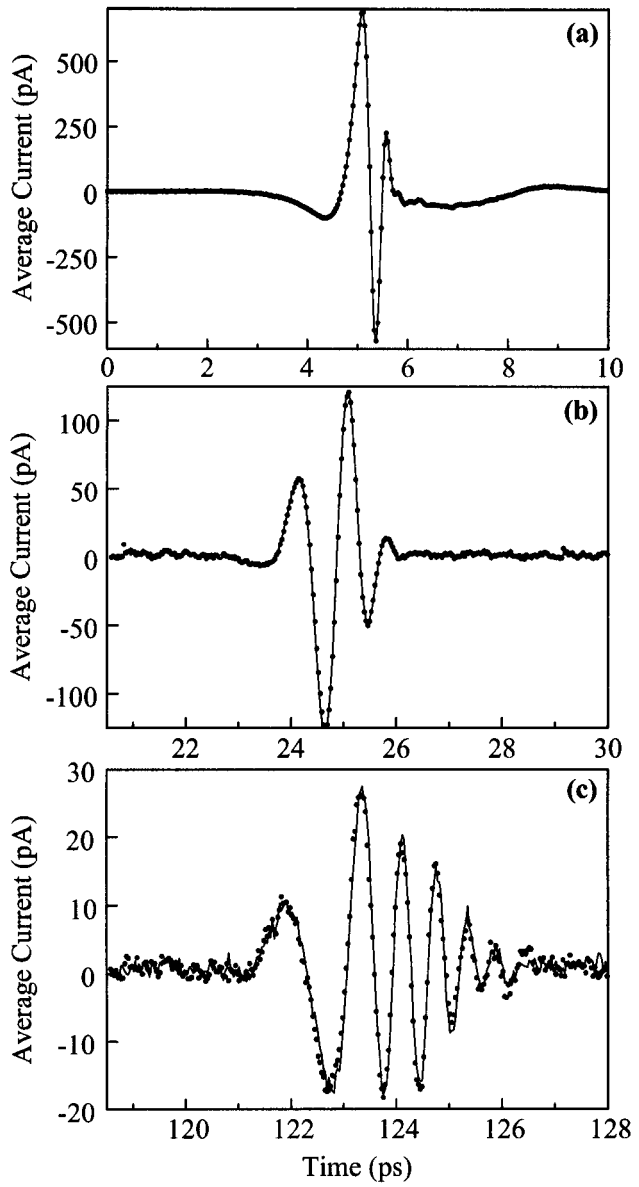

Figure 6. Measurement (dots) and calculation (solid line) of the pulse shape of (a) the excitation pulse (b) the first and (c) the sixth commensurate echo on a magnified time scale for the 10 hPa of methyl fluoride vapor data presented in Figure 3b.

is abolished, and an additional small line shift with increasing K is observed. Both these effects cause an anharmonicity in the line spacing and thereby a gradual dephasing of the individual transitions which is then found as a change in the echo shape.[13,14] An additional effect contributing to pulse reshaping is that for molecules with different isotopes, as is the case for methyl chloride and methyl bromide, slightly shifted rotational spectra of the isotopes are observed that manifest themselves in the time domain as independent sets of echoes, gradually separating from each other with increasing time delay.

Pulse shaping also occurs under conditions where the spectral peak absorption (see Figure 7a) is much larger than unity, and propagation effects strongly affect the observable pulse structure. On an absorption line the gas is a spectrally thick sample with an amplitude attenuation as large as 3000 times. An individual line has a spectral width that is only determined by collisional broadening. As long as the adjacent lines do not overlap and their widths increase linearly with pressure, the peak absorption is independent of the pressure. However, in the transmitted spectrum through a spectrally thick medium the absorption lines appear to be strongly broadened, which in the time domain is

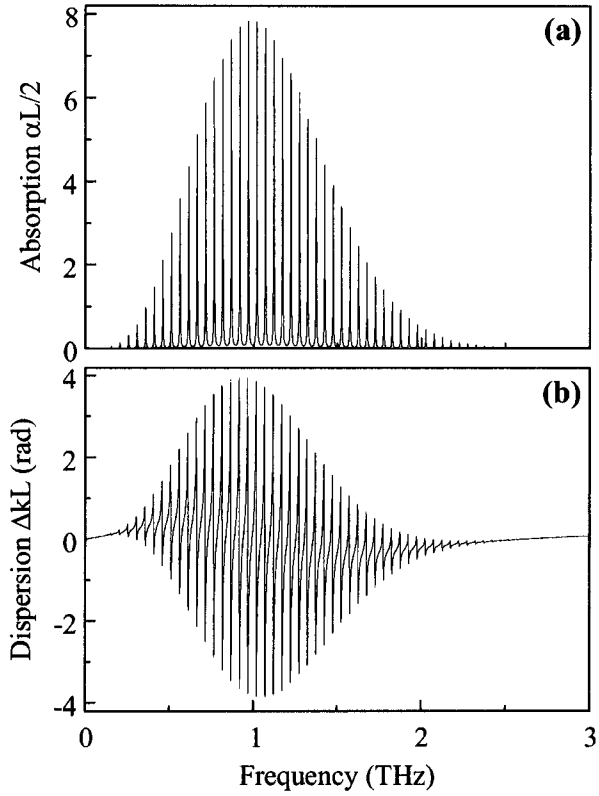

Figure 7. (a) Calculated absorption and (b) dispersion in radians of 22.5 cm of 10 hPa of methyl fluoride vapor.

found as a faster decay of the echoes than expected from collisional dephasing.

Inherently combined with the absorption of the vapor is the dispersion, which in the vicinity of the rotational lines differently delays the frequency components of the THz pulse and by this changes the observable pulse structure. The main contributions of the pulse reshaping and echo decay, illustrated in Figure 6, can be attributed to these propagation effects. Using the theoretical approach to be described below the calculated pulse shapes of the coherent transients are shown as the solid lines in Figures 6a−c. The nearly complete overlap of measured and calculated pulse shapes is obtained when fitting the pulse structure using the rotational and centrifugal stretching constants presented in Table 1 and the line-width distribution shown in Figure 11.

IV. Theory

A quantitative analysis and interpretation of the data requires a precise modeling of the pulse interaction and particularly the response of the molecular vapor. In this section we briefly review the pulse propagation through a sample in terms of linear dispersion theory, we discuss the significance of line shapes for studies of molecular collisions on the basis of the classical line-shape theories of Lorentz and van Vleck−Weisskopf,[5] and we present our new molecular response line-shape theory which includes the time response of molecules orienting to an external field in the presence of collisions.

1. Pulse Propagation. An accurate description of the pulse propagation requires the solution of the coupled Maxwell−Bloch equations, which under certain conditions can be solved by introducing the pulse area concept.[12] Because the THz pulses have a bandwidth comparable with the frequencies of the spectral distribution, it is not appropriate to describe them by a carrier and a time-dependent envelope as is usually done in the infrared and optical regions. This precludes the use of the pulse

TABLE 1: Molecular Parameters Used in the Theoretical Comparisons to the Measurements[a]

gas	$CH_3{}^{79}Br$	$CH_3{}^{81}Br$	$CH_3{}^{35}Cl$	$CH_3{}^{37}Cl$	$CH_3{}^{19}F$
isotope (%)	(50.6)	(49.4)	(75.4)	(24.6)	(100)
μ (D)	(1.797)	(1.797)	(1.869)	(1.869)	(1.790)
A_V (GHz)	(150)	(150)	(156.05)	(156.445)	(154)
B_V (GHz)	9.565	9.528	13.289	13.083	25.524
	(9.56819)	(9.53184)	(13.292876)	(13.088129)	(25.53612)
D_J (kHz)	9	9	17.9	17.2	59.0
	(10.0)	(10.0)	(18.089)	(17.72)	(59.0)
D_{JK} (kHz)	128	128	150	90	445.0
	(128)	(128)	(198.764)	(193.67)	(445.0)
τ_c (fs)			220	220	190

[a] The values in parentheses are the tabulated values (see, e.g., ref 1); the other values are determined by a best fit to the experiment. The electric dipole moments μ are converted into SI units when multiplied by 3.33×10^{-30} A s m.

area concept for pulse propagation effects, and also the slowly varying envelope approximation cannot be applied for pulses essentially consisting of a single cycle.

However, under our low-power conditions we can assume a linear response of the sample to the excitation pulses. Then, the Maxwell−Bloch equations reduce to those of linear dispersion theory.[12−15] The interaction of the electric field with the medium can be described in the frequency domain by means of the complex propagation constant

$$k(\omega) = k_0 + \Delta k(\omega) + i\alpha(\omega)/2 \tag{1}$$

where $k_0 = \omega(n/c)$ is the nonresonant wave vector in the sample and n the refractive index outside the material resonances. $\Delta k(\omega)$ describes the frequency-dependent phase change per unit length due to the resonant interaction with the vapor and $\alpha(\omega)$ the power absorption coefficient. The spectral field distribution $E(z,\omega)$ for a plane wave propagating in the z direction through the medium can then be written as

$$E(z,\omega) = E(0,\omega)\exp(ik_0z)\exp[i\Delta k(\omega)z]\exp[-\alpha(\omega)z/2] \tag{2}$$

and the corresponding propagating pulse, consisting of all the frequency components $E(z,\omega)$, is derived by the Fourier transform of eq 2 as

$$E(z,t) = \int_{-\infty}^{\infty} E(0,\omega)\exp[-i(\omega t - k_0z)]\exp[i\Delta k(\omega)z] \times \exp[-\alpha(\omega)z/2]\,d\omega \tag{3}$$

where $E(0, \omega)$ is the spectral distribution of the input pulse given by the Fourier transform

$$E(0,\omega) = (1/2\pi)\int_{-\infty}^{\infty} E(0,t)\exp(i\omega t)\,dt \tag{4}$$

With the spectral response of the vapor known, the propagation of the THz pulses through the vapor is derived by solving eq 3, which rigorously satisfies the wave equation.

For the methyl halides, as symmetric top molecules, each rotational state with total angular momentum P and rotational quantum number J consists of a manifold of $2J + 1$ sublevels, associated with the projection of the angular momentum P_z on the molecular symmetry axis and indicated by the projection quantum number K. Excitation of the molecular vapor by the THz radiation induces transitions between pairs of J,K levels of the lowest vibrational state. Since for a symmetric top there exists no dipole moment perpendicular to the symmetry axis, no torque along this axis is associated with radiation and therefore no angular momentum changes occur along this axis. Because of this selection rule only transitions from J,K to $J+1,K$ will be observed, and the absorption coefficient for such a transition, assuming unpolarized and/or unoriented molecules, can be calculated (for details see ref 1):

$$\alpha_{JK}(\omega) = C_{JK}\omega g_\alpha(\omega,\omega_{JK}) \tag{5}$$

where $g_\alpha(\omega, \omega_{JK})$ is a general absorption line-shape function of the form

$$g_\alpha(\omega,\omega_{JK}) = \frac{\Delta\omega_J}{(\omega-\omega_{JK})^2 + (\Delta\omega_J/2)^2} f_\alpha^+ - \frac{\Delta\omega_J}{(\omega+\omega_{JK})^2 + (\Delta\omega_J/2)^2} f_\alpha^- \tag{6}$$

It differs from the standard Lorentzian form by being multiplied by an additional shape factor, the switching function f_α^+ for the positive resonance term and a similar factor f_α^- for the "negative" frequency resonance term. For $f_\alpha^\pm = 1$, eq 6 is a pure Lorentzian, while for $f_\alpha^\pm = \pm\omega/\omega_{JK}$ it represents a van Vleck−Weisskopf shape. It is to be noted that, in either the van Vleck−Weisskopf or the Lorentzian limit, the line shape is determined by the collisional dephasing time T_2 as the mean time between collisions, which for the further distinction of individual transitions is replaced by $\tau_J = 2/\Delta\omega_J$, where $\Delta\omega_J$ as the J-dependent fwhm angular frequency line width is assumed to be identical for different K transitions. Only the switching functions, derived in section IV.3 by molecular response theory, involve the collision parameter τ_c. The transition frequency is equal to

$$\omega_{JK}/2\pi = 2(J+1)(B_V - D_{JK}K^2) - 4D_J(J+1)^3 \tag{7}$$

and the quantity C_{JK} is given by

$$C_{JK} = \frac{\pi f_0\mu^2}{3nc\epsilon_0 h}\frac{N_a p}{N_a kT + Bp}(1-\exp[-h\omega_{JK}/2\pi kT]) \times \left(J+1-\frac{K^2}{J+1}\right)\frac{S_W(I,K)}{4I^2+4I+1}\frac{hB_V}{kT}\sqrt{\frac{hA_V}{\pi kT}} \times \exp[-h(B_V J(J+1) + (A_V - B_V)K^2)/kT] \tag{8}$$

B_V and A_V are the rotational constants of the vibrational state about the total angular momentum and symmetry axis, D_J and D_{JK} are the respective centrifugal stretching constants, p is the gas pressure, B is the virial coefficient correcting the number density of a real gas, f_0 is the fraction of molecules in the lowest vibrational state, μ is the electric dipole moment, $S_W(I,K)$ is the statistical weight of a J,K level, I is the nuclear spin of a hydrogen atom, N_a is Avogadro's constant, h is Planck's constant, kT is the thermal energy, c is the speed of light, and ϵ_0 is the vacuum permittivity.

The change of the wave vector is given by

$$\Delta k_{JK}(\omega) = 2C_{JK}\frac{\omega\omega_{JK}}{\omega_{JK}^2 - \omega^2}g_K(\omega,\omega_{JK}) \quad (9)$$

where $g_K(\omega, \omega_{JK})$ is a general dispersion line-shape function of form

$$g_K(\omega,\omega_{JK}) = 1 - \frac{\Delta\omega_J^2}{8\omega_{JK}}\left[\frac{\omega_{JK}+\omega}{(\omega_{JK}-\omega)^2 + (\Delta\omega_J/2)^2}f_k^+ + \frac{\omega_{JK}-\omega}{(\omega_{JK}+\omega)^2 + (\Delta\omega_J/2)^2}f_k^-\right] \quad (10)$$

and $f_k^{\pm}$ is the respective switching function (presented in section IV.3) of the dispersion.

The absorption $\alpha(\omega)$ and dispersion $\Delta k(\omega)$ over the spectral range of the THz pulse is found by summing over all rotational transitions.

$$\alpha(\omega) = \sum_{J=0}^{\infty}\sum_{K=0}^{J}\alpha_{JK}(\omega) \quad (11)$$

$$\Delta k(\omega) = \sum_{J=0}^{\infty}\sum_{K=0}^{J}\Delta k_{JK}(\omega) \quad (12)$$

2. Line-Shape Considerations. In the far-infrared, collisional broadening is by far the most dominant effect in determining the breadth of a spectral line. Also, at infrared and higher frequencies even at comparatively low pressures, collisions strongly affect the width and shape of a spectral line. While the central part of the line shape for a collision-broadened line is predominantly determined by the statistical interruptions of the phase of an atomic or molecular oscillator, with the line width given by the average time between collisions, the shape, particularly in the far wing of a line, is also influenced by the molecular dynamics during a collision. Therefore, line-shape studies may give some deeper insight into the actual collision process itself.

A relatively small but quite fundamental modification of the line shape can be expected from the response of an oscillator to an external field in the presence of collisions. In the basic theories of Lorentz and van Vleck−Weisskopf for collision-broadened lines this response was only considered in its two limiting cases. While Lorentz assumed that directly after a collision molecules are oriented randomly with respect to the driving field and therefore no macroscopic polarization in the sample will be found,[4] van Vleck and Weisskopf applied Boltzmann's statistics,[5] which favors orientations or phases in which molecules are so oriented as to have a low energy in the field. Our further discussion on line-shape investigations will focus on these systematic differences and show that THz-TDS spectroscopy can distinguish between these two fundamental limits.

If a collision is strong enough that the molecule has no further memory regarding its orientation or phase before the collision, and if the collision duration is short enough compared to the period of oscillation of the field, directly after the impact the molecules can be regarded as distributed in accordance with the Boltzmann law appropriate to the instantaneous value of the field. This is known as the adiabatic hypothesis in the van Vleck−Weisskopf theory.[5] However, when the oscillations of the field become faster than the collision duration time or faster than any time response of molecules to the impressed field, no thermalization can be established over the collision, and the original approximation of Lorentz becomes more realistic.

The frequency range where the transition between the two theories occurs indicates the duration of the collision or the molecular response time. This frequency range is completely covered by the spectrum of the THz pulses. Since any orientation of molecules to the field is correlated with some small absorption of this field even far away from any molecular resonance, it can be measured by THz-TDS spectroscopy. The faster the response of molecules, the more this absorption is shifted to the far wing of a line. In any case it should be noticed that any temporal response or redistribution of molecules to the peak THz pulse electric field, which is less than 20 V/m, can only be measured while collisions take place, since they are inducing sublevel transitions and thereby allow for changes of the orientation of a molecule.

Relatively near the resonant line and out to as much as 30 line widths away, our measurements satisfy the condition required by van Vleck and Weisskopf. However, as the offset is further increased this condition is violated, and the Lorentzian approach becomes applicable. In our earlier study of the far wings of resonant lines,[16] we obtained an excellent fit to our measurements by using the van Vleck−Weisskopf theory for the relatively near wings and using an empirically determined weighting function to switch to the Lorentz theory for the far wings.

For this fit,[16] we assumed a simple superposition of the line-shape functions of the van Vleck−Weisskopf and the Lorentz theories for both the power absorption coefficient α_{JK} and the phase shift per unit length $\Delta k_{JK}(\omega)$ for each transition from $J,K \rightarrow J+1,K$ as given by

$$\alpha_{JK}(\omega) = S(\omega)\alpha_{JK}^{VW}(\omega) + (1 - S(\omega))\alpha_{JK}^{L}(\omega) \quad (13)$$

$$\Delta k_{JK}(\omega) = S(\omega)\Delta k_{JK}^{VW}(\omega) + (1 - S(\omega))\Delta k_{JK}^{L}(\omega) \quad (14)$$

The experimental data were well fit by an empirically derived weighting function $S(\omega)$ controlling the transition from the van Vleck−Weisskopf at low frequencies to the Lorentz theory at higher frequencies; this function is given by

$$S(\omega) = (1 + (\omega\tau_c)^2)^{-1} \quad (15)$$

where τ_c is the collision parameter. Equations 13−15 show that the absorption coefficient $\alpha_{JK}^{VW}(\omega)$ and phase shift Δk_{JK}^{VW} of van Vleck−Weisskopf theory are obtained when the parameter $\omega\tau_c \ll 1$ and $\alpha_{JK}^{L}(\omega)$ and Δk_{JK}^{L} of Lorentz theory for $\omega\tau_c \gg 1$.

It is tempting to associate the collision parameter τ_c with the duration of the molecular collision. However, the mean collision duration time estimated from the collision cross section and thermal velocity is expected to be of the order of 1 ps. In addition, the wing absorption of van Vleck−Weisskopf theory is particularly sensitive to state changing (diabatic) collisions causing any orientation of the molecules to the external field,[5] while the full line width of a rotational line is additionally determined by phase-changing (adiabatic) collisions. Since any orientation of molecules during a collision is expected to be much faster than the average overall collision duration time, we will demonstrate below that τ_c is a measure of the orientation time of molecules due to a collision.

3. Molecular Response Theory. We consider the response of an ensemble of harmonic oscillators to an oscillating electric field, where the phase of the oscillators is randomly interrupted due to the molecular collisions. In addition to the classical collision theories we assume a finite response of the oscillators,

which over the collision interaction time can orient to the external field. The equation of motion for the polarization $P(t) = eNx(t)$ of an ensemble of oscillators with mass m, resonant angular frequency ω_0, and number density N, which are subjected to an oscillating field $E(t) = E_0 e^{i\omega t}$ is given by

$$m(\ddot{P} + {\omega_0}^2 P) = e^2 N E_0 e^{i\omega t} \tag{16}$$

and has the general solution

$$P(t) = \frac{e^2 N E_0 e^{i\omega t}}{m({\omega_0}^2 - \omega^2)} + C_1 e^{i\omega_0 t} + C_2 e^{-i\omega_0 t} \tag{17}$$

When an oscillator has last experienced a collision at time t_0, the transient amplitudes C_1 and C_2 are found from the initial conditions of $P(t_0)$ and $\partial/\partial t\ P(t_0)$ at that time. Since none of the collisions are alike, different oscillators will have different values of $P(t_0)$ and $\partial/\partial t\ P(t_0)$. The average is found from the linear sum of these contributions, which is the same as though one considers a single oscillator with the respective initial conditions.

Assuming positive and negative values of $P(t_0)$ and $\partial/\partial t\ P(t_0)$ as equally probable, so that on the average directly after the collision $P(t_0) = \partial/\partial t\ P(t_0) = 0$, eq 17 becomes

$$P_L(t,t_0) = \frac{e^2 N E_0 e^{i\omega t}}{m({\omega_0}^2 - \omega^2)} \times \left\{1 - \frac{\omega_0 + \omega}{2\omega_0} e^{i(\omega_0 - \omega)(t - t_0)} - \frac{\omega_0 - \omega}{2\omega_0} e^{-i(\omega_0 + \omega)(t - t_0)}\right\} \tag{18}$$

which represents the Lorentz case. In contrast, for the van Vleck−Weisskopf case, it is required that directly after the collision an oscillator is in thermal equilibrium with the field; *i.e.,* the initial conditions have to be in agreement with Boltzmann's distribution law as given by $P(t_0) = e^2 E_0 e^{i\omega t_0}/m{\omega_0}^2$, and $\partial/\partial t\ P(t_0) = 0$. These different initial conditions increase the transient amplitudes C_1 and C_2 by an amount ΔC (for details see ref 5) and can be identified as an additional small polarization term $\Delta P(t)$ which becomes

$$\Delta P(t,t_0) = \frac{e^2 N E_0 e^{i\omega t}}{2m{\omega_0}^2}(e^{i(\omega_0 - \omega)(t - t_0)} + e^{-i(\omega_0 + \omega)(t - t_0)}) \tag{19}$$

This term determines the difference between these fundamental theories, and the extra polarization is expected as long as the collisions are sufficiently rapid, so that the alternations of the field during a collision can be regarded as negligible (adiabatic hypothesis). However, when the field oscillation frequency is so high that the phase oscillates several times within the molecular response time, the collisions become ineffective in creating thermal equilibrium. Then, this extra contribution should disappear, and the system is presumably better described by the Lorentzian assumption. So it is obvious that the amount of $\Delta P(t)$ is determined by the time response of the oscillator with respect to the frequency of this field.

Consider polar molecules which would orient to a step function field with an exponential response proportional to $\Delta P_{th}(1 - e^{-t/\tau_c})$, where ΔP_{th} is the maximum polarization due to thermal equilibrium and τ_c is the molecular response time. The probability for a molecule of becoming aligned to the field within a time increment $d\vartheta$ is $(1/\tau_c)e^{-\vartheta/\tau_c}\ d\vartheta$, where ϑ is the time evolution over the collision. Therefore, the effective polarization in an alternating field may be derived by multiplying eq 19 by this probability and integrating over the collision duration time. As long as this time is short compared to the mean time τ between collisions, the interactions over the collisions can be considered to be independent from the time between collisions, and the effective change in polarization is calculated as

$$\Delta P(t,t_0) = \frac{1}{\tau_c}\int_0^\infty \Delta P(t,t_0 + \vartheta) e^{-\vartheta/\tau_c}\ d\vartheta$$

$$= \frac{e^2 N E_0 e^{i\omega t}}{2m{\omega_0}^2}\left\{\frac{1 + i(\omega_0 - \omega)\tau_c}{1 + (\omega_0 - \omega)^2{\tau_c}^2} e^{i(\omega_0 - \omega)(t - t_0)} + \frac{1 - i(\omega_0 + \omega)\tau_c}{1 + (\omega_0 + \omega)^2{\tau_c}^2} e^{-i(\omega_0 + \omega)(t - t_0)}\right\} \tag{20}$$

Since the collisions in the ensemble occur at random with a mean interval τ, we have to average the whole polarization $P(t,t_0) = P_L(t,t_0) + \Delta P(t,t_0)$ over the various times of last collision, where the probability that the last collision was in the interval $t_0 - dt_0$, t_0 is $(1/\tau)e^{-(t-t_0)/\tau}\ dt_0$. Therefore, eqs 18 and 20 are multiplied by this probability and integrated over t_0 from $-\infty$ to t yielding the overall polarization

$$P(t) = (1/\tau)\int_{-\infty}^{t}(P_L(t,t_0) + \Delta P(t,t_0))e^{-(t-t_0)/\tau}\ dt_0 = \epsilon_0 \chi(\omega) E_0 e^{i\omega t} \tag{21}$$

where $\chi(\omega) = \chi_L(\omega) + \Delta\chi(\omega)$ is the complex electric susceptibility consisting of the Lorentzian contribution with

$$\chi_L(\omega) = \frac{e^2 N}{\epsilon_0 m({\omega_0}^2 - \omega^2)}\left\{1 - \frac{\omega_0 + \omega}{2\omega_0}\frac{1 + i(\omega_0 - \omega)\tau}{1 + (\omega_0 - \omega)^2\tau^2} - \frac{\omega_0 - \omega}{2\omega_0}\frac{1 - i(\omega_0 + \omega)\tau}{1 + (\omega_0 + \omega)^2\tau^2}\right\} \tag{22}$$

and the extra term

$$\Delta\chi(\omega) = \frac{e^2 N}{2\epsilon_0 m{\omega_0}^2}\left\{\frac{1 + i(\omega_0 - \omega)\tau_c}{1 + (\omega_0 - \omega)^2{\tau_c}^2}\frac{1 + i(\omega_0 - \omega)\tau}{1 + (\omega_0 - \omega)^2\tau^2} + \frac{1 - i(\omega_0 + \omega)\tau_c}{1 + (\omega_0 + \omega)^2{\tau_c}^2}\frac{1 - i(\omega_0 + \omega)\tau}{1 + (\omega_0 + \omega)^2\tau^2}\right\} \tag{23}$$

Note that for $\tau_c = 0$ the last equation reduces to the standard correction term in the van Vleck−Weisskopf theory, and $\chi(\omega)$ recovers the van Vleck−Weisskopf case. For finite τ_c values and increasing frequency detunings eq 23 goes to zero, and the overall polarization approaches the Lorentzian case.

It is important to note that the complex terms of the form $A(\omega) = 1/(1 + i\omega\tau) = (1 - i\omega\tau)/[1 + (\omega\tau)^2]$ satisfy the Kramers−Kronig relationship[33] and are the frequency-domain representation of the time-domain response function $\exp(-t/\tau)$, which vanishes for positive argument as required by causality. This relationship describes both the dielectric Debye[34] and the conductive Drude[35] response. In eqs 22 and 23 this function appears with the shifted frequency variables $(\omega - \omega_0)$ and $(\omega + \omega_0)$, corresponding to shifting from zero resonant frequency for Debye and Drude theory to resonances at ω_0 and $-\omega_0$, respectively. These shifted functions also satisfy the Kramers−Kronig relationship and result from the time-domain response functions of the collision process $\exp(-t/\tau_c)$ and the dephasing process between collisions $\exp(-t/\tau)$, both of which vanish for positive argument. The complete result for $\chi(\omega)$ also

satisfies the Kramers−Kronig relationship and is fully consistent with linear response theory.

The extra term resulting from the orientational order established during the collision process as presented in eq 23 has a spectral response that is symmetric with respect to τ_c and τ for both the resonant and antiresonant term. The form of this term is very much like that of the two-parameter Rocard−Powles complex permittivity,[36−38] derived for the nonresonant (zero resonant frequency) case, which is the next higher order approximation after the single-parameter Debye theory.

Indeed, in the zero resonance frequency limit the molecular response theory has the same mathematical form as the Rocard−Powles result which was derived by the inclusion of nonzero molecular inertia into the Debye theory.[36−38] This form of the complex susceptibility is the same as that obtained by a second-order truncation of the Mori continued fraction.[38] Thus, the transition dipole autocorrelation function has a maximum at $t = 0$ with zero slope which can be seen by plotting the zero resonance frequency limit of the susceptibility, $\chi(\omega_{JK} \rightarrow 0)$, on a Cole−Cole plot which shows the imaginary part of $\chi(\omega)$ plotted against the real part. In the high-frequency limit this curve asymptotically approaches the x (real) axis, indicating the correct behavior of the dipole autocorrelation function near zero time.[38] Although the second-order truncation of the Mori continued fraction is an approximation, the experimental results clearly indicate the validity of the molecular response theory over this frequency range. In order to obtain information on higher order convergents, it would be necessary to make accurate measurements over an even broader spectral bandwidth on the far wings of the rotational lines.

When separating the complex susceptibility $\chi(\omega) = \chi'(\omega) - i\chi''(\omega)$ into its real and imaginary part, the above result can be also expressed in the form

$$\chi'(\omega) = \frac{e^2 N}{\epsilon_0 m(\omega_0^2 - \omega^2)} g_K(\omega,\omega_0) \tag{24}$$

$$\chi''(\omega) = \frac{e^2 N}{4\epsilon_0 m\omega_0} g_\alpha(\omega,\omega_0) \tag{25}$$

where $g_K(\omega,\omega_0)$ and $g_\alpha(\omega,\omega_0)$ are the line-shape functions of eqs 6 and 10, and the switching functions using the notation $1/\tau = \Delta\omega_0/2$ are found to be

$$f_k^{\pm}(\omega,\omega_0) = 1 - \frac{\omega_0 \mp \omega}{\omega_0} \frac{1 - 2(\omega_0 \mp \omega)^2\tau_c/\Delta\omega_0}{1 + (\omega_0 \mp \omega)^2\tau_c^2} \tag{26}$$

$$f_\alpha^{\pm}(\omega,\omega_0) = 1 - \frac{\omega_0 \mp \omega}{\omega_0} \frac{1 + \Delta\omega_0\tau_c/2}{1 + (\omega_0 \mp \omega)^2\tau_c^2} \tag{27}$$

These functions control the transition between the two basic line-shape forms of Lorentz and van Vleck−Weisskopf. For a quantum mechanical rotator with the rotational transitions $J, K \rightarrow J, K+1$ the frequency ω_0 and line width $\Delta\omega_0$ in eqs 22−27 are replaced by ω_{JK} and $\Delta\omega_{JK}$ and e^2/m is replaced by $4\pi\omega_{JK}\mu^2/3h$; the number density N is replaced by ΔN, the population difference between rotational levels. The complex susceptibility, $\chi(\omega)$, then determines the propagation constant $k(\omega)$ of eq 1. An inspection of the switching functions shows that in the limit $1 \ll (\omega_{JK} \mp \omega)^2\tau_c^2$, $f_\alpha^{\pm} \rightarrow 1$, and the generalized function becomes the well-known Lorentzian for absorption, while $f_k^{\pm} \rightarrow 1 + (\omega_{JK} \mp \omega)\tau/\omega_{JK}\tau_c$. Conversely, when $(\omega_{JK} \mp \omega)^2\tau_c^2 \ll 1$, $f_\alpha^{\pm}, f_k^{\pm} \rightarrow \pm\omega/\omega_{JK}$ and the van Vleck−Weisskopf line shape is obtained.

This approach provides the first dielectric response function describing such a system, where the response time of the molecules occurs naturally in the theory together with the mean time between collisions. The response approaches that of the van Vleck−Weisskopf or Lorentzian theories in the appropriate limits. Compared to the initial discussion of van Vleck and Weisskopf and the simple empirical model presented in section IV.2, the superposition parameter is not $\omega\tau_c$, but must be replaced by the two parameters $(\omega - \omega_{JK})\tau_c$ and $(\omega + \omega_{JK})\tau_c$.

V. Comparison of Calculations and Measurements

Using the theoretical framework presented in the previous section, an analysis of a measurement can be performed by Fourier transforming the measured pulse structure into the frequency domain and comparing with the theoretical spectra, or the analysis can be done in the time domain by simulating the pulse structure and comparing it directly with the measurement. In both cases, the absorption and dispersion of the vapor have to be calculated from eqs 5−12 with the known molecular constants.

The theoretical amplitude absorption $\alpha(\omega)\ L/2$ and phase change in radians $\Delta k(\omega)L$ for 10 hPa of methyl fluoride with a cell length of $L = 22.5$ cm and $T = 294$ K are shown in Figure 7. These spectra were calculated with the parameters given in Table 1. The values in parentheses are the tabulated values,[1,39,40] which were used as the starting points for our fitting procedure. The values of the molecular constants B_V, D_J, and D_{JK} determined by fits to our measurements are also shown in Table 1. It should be noted that the rotational constants derived from our analysis give slightly smaller values than those of the tabulated values which were determined from measurements at very low pressures. We explain this discrepancy as originating from pressure-induced line shifts of the rotational lines. Since our analysis does not distinguish between individual line shifts, the smaller rotational constants and stretching parameters compensate for an average pressure shift of the rotational spectrum to smaller frequencies. Further parameters used in the calculations for the methyl fluoride spectra are the fraction of molecules in the lowest vibrational state ($f_0 = 0.986$ at 294 K), the J-dependent line width, shown in Figure 11, and the nonresonant refractive index change with pressure, $dn/dp = 4.3 \times 10^{-7}$/hPa.

The theoretical absorption and dispersion of the vapor can then be compared with the respective spectra derived from the THz-TDS measurements. However, when the peak absorption is much larger than unity (see Figure 7a) and frequencies at the band center are strongly attenuated (about 3000 times) down to a level almost comparable with the noise, small-amplitude fluctuations cause large uncertainties in the spectral absorption coefficient. Due to the equivalence of the time-domain and frequency-domain data via the Fourier transform, we prefer an analysis of the measurements by directly comparing them with a calculated pulse structure in the time domain, especially for a spectrally dense medium.

Our calculations are strictly numerical and are performed in the following manner. The measured reference pulse (Figure 3a) is assumed to be the input pulse to the vapor. Its numerical Fourier transform $E(0,\omega)$ is then multiplied by the theoretical amplitude absorption and dispersion, derived from eqs 5−12 and shown in Figure 7. Finally, the inverse numerical Fourier transform of eq 3 is performed to obtain the predicted output pulse. The final analysis is done by fitting the simulated structure to the measurement which determines the molecular constants B_V, D_J, and D_{JK} given in Table 1. The result of our numerical analysis for 10 hPa of methyl fluoride is the predicted

pulse train shown in Figure 3c and on an expanded time scale in Figure 6 as the solid curves. We have good agreement with the measurement in both pulse shape and amplitude for the transmitted excitation pulse as well as the commensurate echoes.

Obtaining a good fit to low-pressure data, i.e., 10 hPa, permits accurate determination of the constants shown in Table 1 due to the large number of commensurate echoes which extend to hundreds of picoseconds. For the rotational constant, B_v, the values used in our fitting procedure agrees with the published values to almost four decimal places. These constants are then used as initial values in fitting the high-pressure data where collisional dephasing causes a rapid decay of the coherent transients.

Further comparisons between theory and our THz-TDS experiments will focus on two aspects of this investigation. The first is measurements at high pressures which permit detailed investigation of the line shape. By measuring the transmitted THz spectrum at higher pressures, the experiment becomes highly sensitive to the far-wing absorption of the rotational lines. An accurate fit of the far-wing line-shape profile allows us to accurately determine the molecular orientation time τ_c used in the theory of section IV.3. The second aspect of this investigation is the empirical determination of the J-dependent dephasing times τ_J (related by $2/\Delta\omega_J$ to line width in the frequency domain) for a wide range of pressures.

1. Line-Shape Investigations at Higher Pressures. Propagation effects become very significant at increased pressure since a broader spectral range is affected by the phase shifts. This is demonstrated by Figure 8, which shows measurements of methyl fluoride for three different vapor pressures. For 10 hPa the transmitted excitation pulse has only been slightly attenuated and reshaped with the echo pulse train extending to beyond 200 ps. When the pressure is increased to 100 hPa, the peak-to-peak amplitude of the transmitted driving pulse is reduced to approximately one-half of its initial value and the pulse is significantly reshaped. The relatively larger echo pulse train decays much more rapidly, and compared to the 10 hPa results the echoes are strongly reshaped. At 1000 hPa the transmitted driving pulse is severely attenuated and reshaped; only four echoes are easily observable.

The reshaped pulse at 1000 hPa pressure is shown on an expanded time scale in Figure 9a and compared to theory; the agreement is excellent and both lines completely overlap. The transmitted excitation pulse is completely reshaped due to both the strong absorption and dispersion of the vapor. The pulse has broken up and shows a fast beating on the leading edge, while the lower frequencies are shifted to the trailing edge. This produces a significant negative chirp over the pulse envelope due to the net negative dispersion in the vapor at high frequencies and positive dispersion at low frequencies. The first echo has been stretched out and appears as a simple wave packet. Figure 9b compares the transmitted spectrum with the input (reference) spectrum and shows that in the center the vapor is completely opaque while it becomes partially transparent in the low- and high-frequency wings. For frequencies larger than 2.5 THz almost no further absorption is observed.

For the 1000 hPa of methyl fluoride measurement the amplitude absorption $\alpha(\omega)L/2$ is obtained from the data of Figures 3a and 8c. The theoretical absorption is shown for the entire rotational band in Figure 9c and falls completely within the bandwidth of the reference spectrum shown in Figure 9b. Measurement of the amplitude absorption on the high-frequency wing is compared to that calculated from the van Vleck−Weisskopf line shape and the new molecular response theory using a collision-induced orientation time of $\tau_c = 190$ fs and is

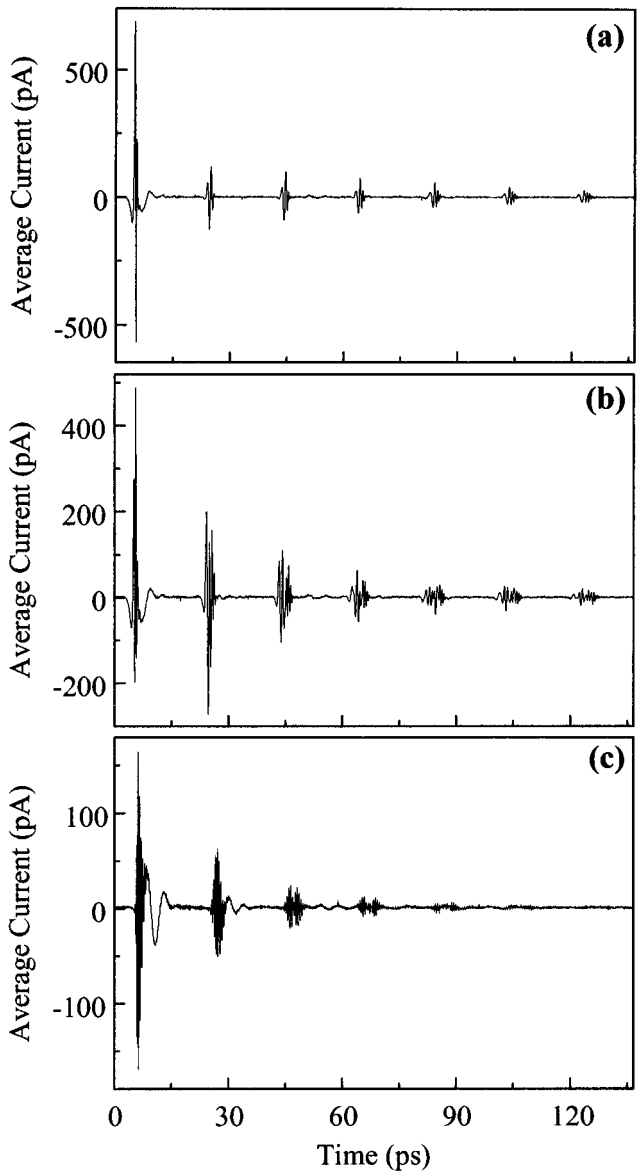

Figure 8. (a) Measured transmitted THz pulse through 22.5 cm of 10 hPa of methyl fluoride vapor. (b) Measured THz pulse through 100 hPa of vapor. (c) Measured THz pulse through 1000 hPa of vapor.

shown in the inset to Figure 9c. The measurement and calculation using our molecular response theory agree quite well, while the absorption based on the van Vleck−Weisskopf profile (upper curve) is clearly too large. Variation of the fitting parameters indicate an uncertainty of 30% for the collision parameter, τ_c.

When the 22.5 cm sample cell is filled with 2026 hPa of methyl chloride vapor, as shown in Figure 10a, the reshaped and attenuated excitation pulse is followed by a series of coherent transients, which rapidly decay because of the strong collisional broadening. The reshaped first coherent echo of Figure 10a is displayed as individual data points on an expanded time scale in Figure 10b, where the dramatic reshaping can be seen in detail. Figure 10c shows the calculated absorption compared to the reference spectrum—again the THz pulse bandwidth is much larger than the absorption of all states populated at room temperature. The disagreement between the measured absorption and that calculated using the van Vleck−Weisskopf and the Lorentz line shapes is shown for the high-frequency wing in Figure 10d. It is clear that the actual absorption falls between that predicted from the van Vleck−Weisskopf and Lorentz theories. However, the absorption

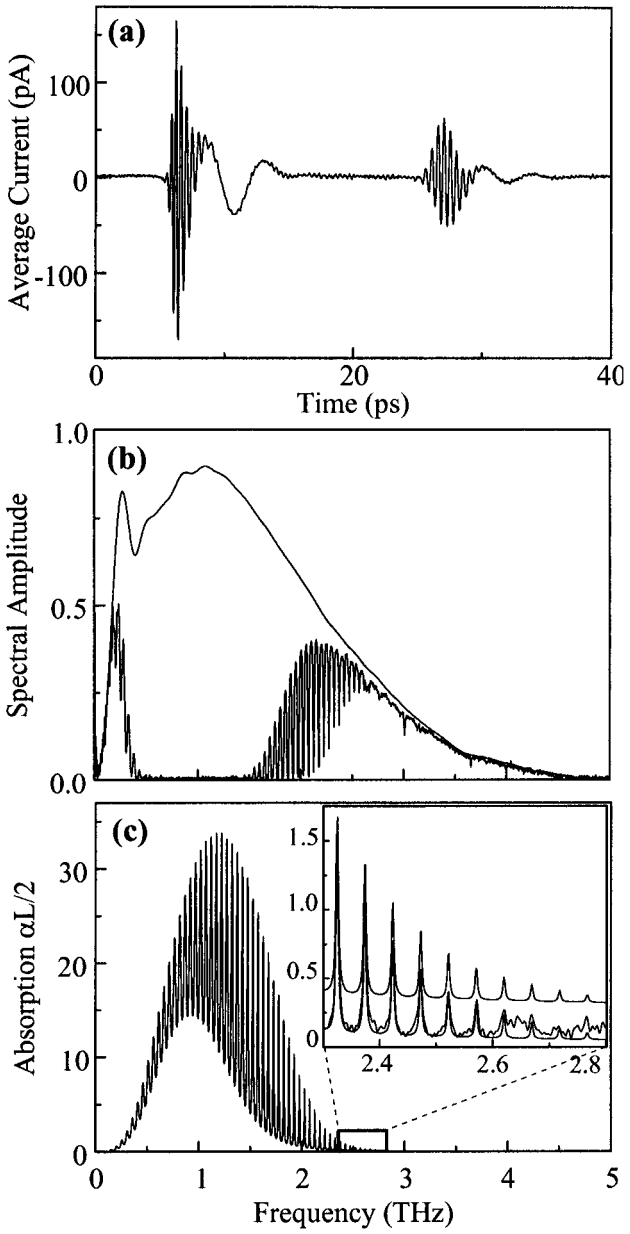

Figure 9. (a) Calculated (dashed line) and measured (solid line) transmitted THz pulse through 1000 hPa of methyl fluoride vapor. (b) Amplitude spectrum of reference pulse compared with transmitted spectrum. (c) Calculated absorption of 1000 hPa, 22.5 cm long methyl fluoride vapor. The inset shows the experimental far-wing absorption compared to that calculated for the van Vleck−Weisskopf line shape (upper curve) and for the molecular response theory (lower curve).

calculated by molecular response theory and shown as the dashed line completely overlaps the measured data on the far wing. The overlap of experiment and theory confirms the validity of molecular response theory and clearly demonstrates its applicability between the two limiting cases of the Lorentzian and van Vleck−Weisskopf theories.

Quantitative evaluation in the time domain using our molecular response theory for 2026 hPa of methyl chloride is performed in a manner similar to that discussed above for methyl fluoride. The simulated pulse structure is compared with the measurements in Figure 10a,b. In contrast to the Lorentz and van Vleck−Weisskopf line shapes, the molecular response theory gives excellent agreement with the measurement. The pulse structure calculated for the first echo using a collision parameter of $\tau_c = 220$ fs is shown as the solid line in Figure 10b, while that calculated with a van Vleck−Weisskopf line shape is shown as a dashed line. The strong far-wing absorption

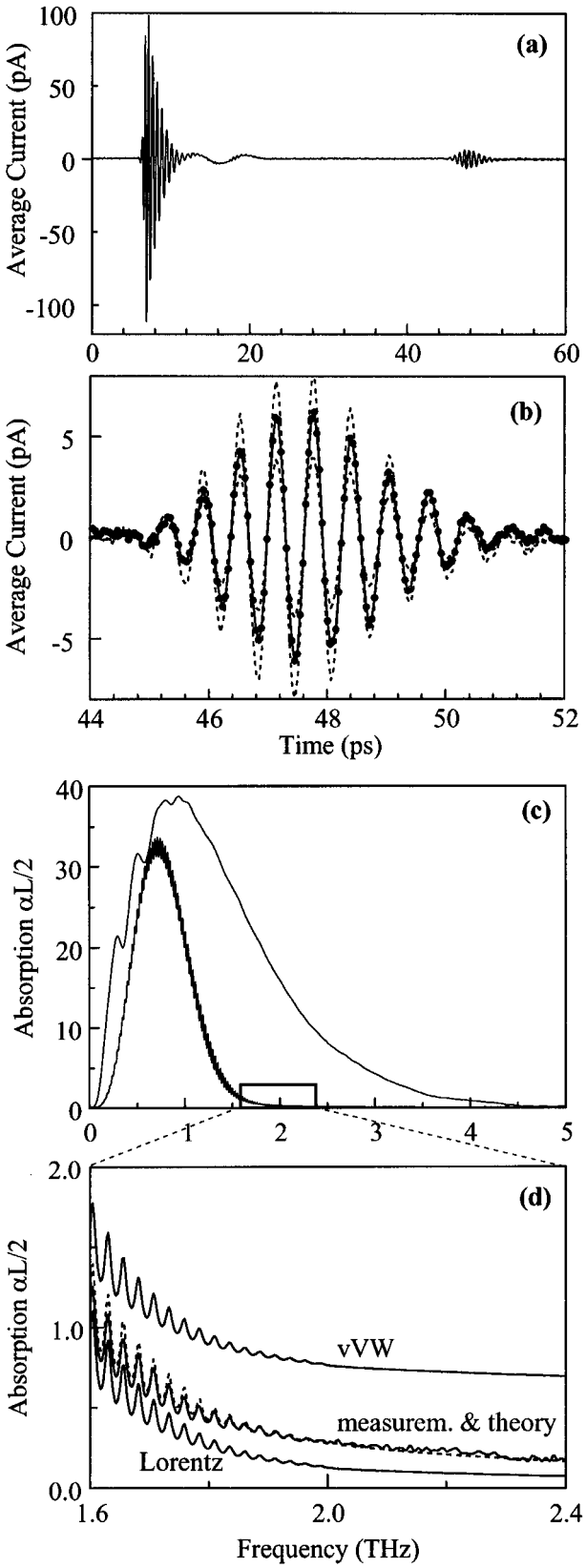

Figure 10. (a) Measured (solid line) and calculated (dashed line) transmitted THz pulse for 2026 hPa of methyl chloride vapor. There is complete overlap of the traces. (b) Measured (points) and calculated first THz commensurate echo pulse on an expanded time scale for the Lorentz (upper dashed line), molecular response (solid line), and van Vleck−Weisskopf (lower dashed line) line shapes. (c) Calculated absorption of 2026 hPa, 22.5 cm long methyl chloride vapor compared to the reference spectrum of the input pulse. (d) Experimental far-wing absorption compared to that calculated for the van Vleck−Weisskopf line shape (upper curve), for the Lorentz theory (lower curve) and for molecular response theory (dashed line).

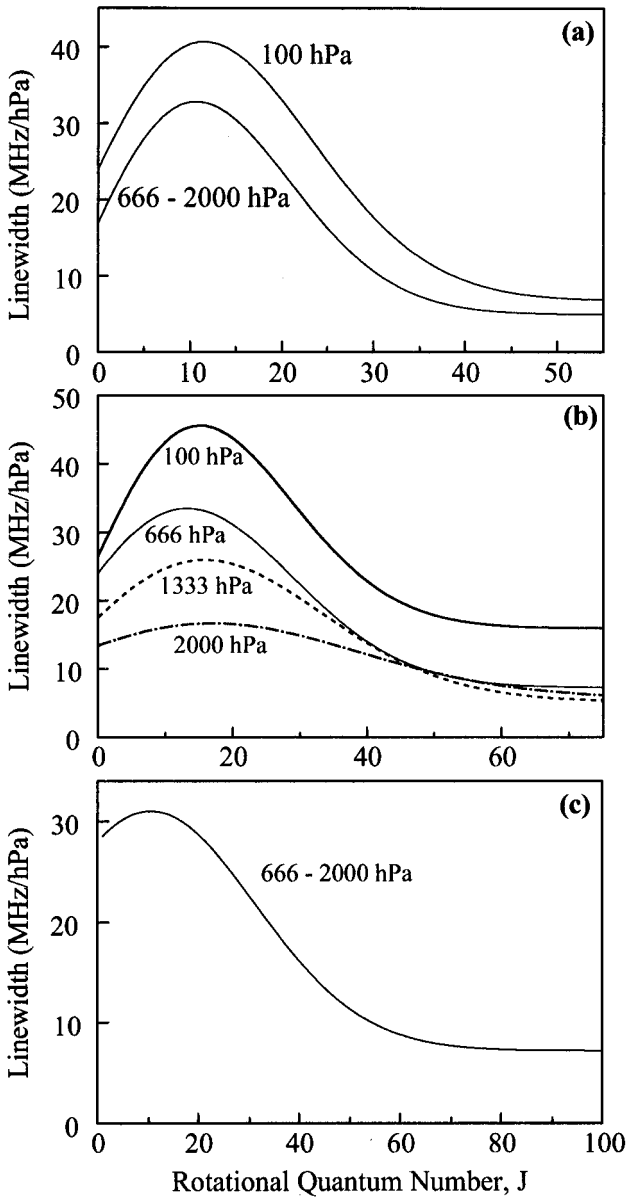

Figure 11. Experimentally determined *J*-dependent line width for (a) methyl fluoride, (b) methyl chloride, and (c) methyl bromide.

results in underestimation of the pulse amplitude. Calculations of the echo shape using the Lorentz line shape (also shown as a dashed line in Figure 10b) overestimates the echo amplitude. Only the molecular response theory (the solid line) is in complete agreement with the data points. The uncertainty of the response time is again ±30%.

2. J-Dependent Line Width. In addition to the pulse reshaping due to propagation effects at high pressures, we observe further reshaping due to the variation of the line width with the rotational quantum number *J*. In order to determine as precisely as possible the *J* dependence of the line shape, we used a short cell of length 2.27 cm for pressures above approximately 600 hPa. The short path length gives us sensitivity to the line shape across the entire rotational band manifold as is seen in Figure 5. This contrasts to previous measurements in longer cells where there was complete occlusion at the center of the band (for example, Figure 9b).

The empirically determined *J*-dependent broadening distributions used in fitting the data obtained from the short cells are shown in Figure 11. The 100 hPa data curves were obtained using the 22.5 cm cell. At pressures below 100 hPa in methyl chloride and methyl fluoride, the individual line widths are assumed to increase linearly with pressure and can then be expressed by the line width $\Delta\omega_J = 2\pi C_J p$, where C_J is the distribution shown in Figure 11 for 100 hPa. The experimentally realized delay time was not long enough to measure or confirm this line width distribution for pressures of 10 hPa or less. At these low pressures a reshaping of the echoes due to a changing line width can only be observed at delay times larger than 1 ns. However, the average broadening and by this the average relaxation time T_2 is determined quite accurately from the damping of the echoes. Since the decay of the echoes is well represented by the distribution of Figure 11, we assume the same dependence at low pressures for methyl fluoride and chloride. Measurements were not conducted in methyl bromide below 666 hPa.

At pressures above 100 hPa, however, changing distributions for the line width and a strong nonlinear broadening with vapor pressure can be observed, indicating that at higher pressures, ternary and other multiple collision effects become important. All the distributions shown in Figure 11 were obtained from our time-domain fitting procedure and can be represented by an empirically derived formula[15]

$$C_J = C_0\left(r + (1-r)\frac{J+A}{A}\exp(-J^2/\Delta^2)\right) \qquad (28)$$

which has a similar dependence on *J* as the absorption coefficient (eqs 5 and 8). Equation 28 takes into account that the part of the broadening due to resonant collisions is proportional to the number of molecules in the states involved. In eq 28, C_0 is the broadening parameter of the reference transition $J = 0 \rightarrow J = 1$ given in MHz/hPa, *r* describes the remaining width at large *J*'s as the fraction of the initial width, and *A* and Δ determine the amplitude and width as well as the maximum position of the distribution. The parameters giving the linewidth variation of Figure 11 are listed in Table 2.

It is important not to overinterpret the accuracy of the *J*-dependent broadening parameters used in our fits. Although it is clear that the functional form of C_J necessary to fit the THz-TDS data within our experimental error is that shown in Figure 11, variations of the fitting parameters of eq 28 on the order of 10% also lead to acceptable fits. This is especially true at low *J* values where the reduced THz beam intensity and low population in the rotational states significantly reduce the sensitivity of the fit. Our fits for the *J*-dependent broadening parameters are quite accurate on the high-frequency wing of the rotational absorption band as long as the line shape is clearly visible as seen in Figures 5, 9c, and 10c.

TABLE 2: Empirically Determined Values of the Parameters Used To Determine the *J*-Dependent Line Width in Eq 28 for Room Temperature

gas	CH_3F			CH_3Cl				CH_3Br		
press. (hPa)	100	666	2000	100	666	1333	2000	666	1333	2000
C_0 (MHz/hPa)	24	17	17	26.5	24	17.5	13.4	28	23	26
r	0.28	0.29	0.29	0.61	0.3	0.3	0.42	0.26	0.29	0.26
Δ	20.5	18.1	18.1	24.6	26.3	30.1	36.4	32	34	32
A	6.8	4.7	4.8	4.9	13	13	22.4	38	37	40

VI. Conclusion and Future Directions

Using the technique of THz-TDS, we have experimentally and theoretically studied methyl fluoride, chloride, and bromide vapor over a wide range of pressures. After excitation by a single subpicosecond pulse of THz electromagnetic radiation, the vapor sample was observed to emit a train of subpicosecond THz pulses. Pulse reshaping of these THz commensurate echoes with increasing time resulted from the anharmonicity in the line spacing due to centrifugal stretching, the absorptive and dispersive propagation effects, a varying line width broadening over the rotational spectrum, and the isotopic composition of the vapor. Under the conditions of low pressure a linear dispersion theory analysis was used to obtain the frequency separation between the individual methyl halide lines and the centrifugal stretching constant. Using the constants obtained from the low-pressure results allows an empirical determination of the *J*-dependent line width under conditions of high pressure and short optical path lengths. Our measurements show a strong nonmonotonic *J* dependence for the collision broadening coefficient.

Under conditions of high pressure and long cell length, a large discrepancy was observed on the far wings of the line between the measurements and calculations using either the van Vleck−Weisskopf or the Lorentzian line shape. To explain these discrepancies, it is necessary to use a line-shape theory which explicitly includes the molecular orientation time during a collision. Such a molecular response theory has been developed within the framework of van Vleck−Weisskopf and Lorentz and reduces to these in the appropriate limits. This molecular response theory is applicable to the transition region between the van Vleck−Weisskopf and Lorentz theories where the frequency detuning from resonance is of the same magnitude as the orientation rate. Although there are several theories[41,42] that consider line broadening from the calculations of interaction forces during a collision and predict variations from the Van Vleck−Weisskopf and Lorentz line shapes, the only new parameter introduced by the molecular response theory is a molecular reorientation time during the collision, τ_c. The good agreement obtained between measurement and calculations incorporating this new line shape, especially for the far-wing absorption, is significant considering that the intermolecular potentials are not required.

The driving force behind our investigation of the commensurate echoes in molecular vapors[13−16] has been the high dynamic range of the THz time-domain spectroscopy data. The high signal-to-noise ratio allowed accurate data to be obtained from on resonance to frequency offsets of over 5 times the resonant frequency of the rotational transitions in the far wings and forced the development of the molecular response theory presented here.

The ability to accurately measure molecular interactions through their far-infrared absorption and dispersion over a wide range of experimental conditions should have far-reaching importance. In fact, THz spectroscopy using very short path lengths has recently looked at the response of polar and nonpolar molecules in the liquid phase,[43−45] illustrating the capability for analysis of very dense samples. One example of dense sample studies would be laboratory simulations of spectroscopy of the planetary atmospheres mentioned in the Introduction. Another area of investigation in the category of a difficult sample is the THz characterization of saturated water vapor up to high pressures of several atmospheres having applications in understanding electromagnetic propagation in the atmosphere. A particular feature for investigation would be the appearance of new resonant transitions, indicating the formation of water complexes since clusters of water molecules existing in nonequilibrium conditions have been predicted to be responsible for anomalous atmospheric absorption in the submillimeter[46] and 8−14 μm regions of the spectrum.[47] Water dimers have been experimentally observed in molecular beams and found to have substantial dipole moments of the order of 2.6 D,[48] making them amenable to detection by THz-TDS. Water dimers, trimers, and higher polymers of various configurations are also of interest in studies of water droplet nucleation which has application to gaseous pollutant removal.[49]

THz-TDS is very well suited for other types of samples that are problematic for other far-infrared spectroscopy techniques, for example, hot samples such as flames.[50] Unlike measurements utilizing fixed frequency FIR lasers, the bandwidth of THz-TDS can extend continuously over the wide spectral range from 0.1 to greater than 6 THz, permitting the simultaneous detection of many species. Compared to Fourier transform spectroscopy, the THz radiation sources generate well-collimated, low-divergence beams which are of advantage in working with flames. The room-temperature, coherent THz receiver is 1000 times more sensitive to THz (far-infrared) radiation than a liquid helium cooled bolometer. Furthermore, the gated coherent detection used in THz-TDS is insensitive to the copious thermal background radiation emitted by the flame, which would overdrive a bolometer.

The first comprehensive far-infrared absorption measurement of flames covered the region from 7 to 88 wavenumbers (0.2 to 2.65 THz) and identified a large number of absorption lines—including those of water, CH, and NH_3—in a premixed propane:air flame.[50] The measured absorption strength permitted the determination of species concentration along the beam path, while the flame temperature was determined by comparing the relative strengths of the water vapor lines. The sensitivity of THz-TDS to free charges makes it a promising candidate to examine the role that the difficult-to-measure ionized species[51] play in flames. These species are hypothesized to play an important role in the formation of soot.[52] Although still poorly understood, soot generation has received much attention both from the importance of soot as a pollutant and since sooting flames have been demonstrated to produce large carbon clusters such as fullerenes.[53]

Coherent THz pulse propagation studies, similar to those of low-intensity 0π pulse propagation for the optical case,[12,54−58] would also be of interest. Compared to studies of coherence effects in the radio-frequency and microwave regimes for nuclear and electron spin systems, the THz experiments would involve samples many wavelengths in length, so that in addition to the point response propagation effects would also be important. In contrast to investigations at infrared and optical frequencies, where coherent transients are usually detected as pulse intensities or as beat notes on a carrier,[59−61] the THz experiments would directly measure the actual electric field of the transmitted radiation pulse and that radiated by the coherent response of the sample. Because the THz pulse does not have a carrier frequency and is composed of a broad frequency band for which the frequency changes by more than 50 times from the lowest to highest values, it is not appropriate to describe these pulses in the usual way by a carrier frequency and a time-dependent envelope.[12] Therefore, the powerful concept of pulse area and the slowly varying envelope approximation of coherent optics cannot be applied for pulses that essentially consist of a single cycle. It is not clear whether self-induced transparency can even occur under these conditions. Thus, THz pulse propagation effects will require different concepts for their understanding. For dense resonant vapors exceptionally slow

THz pulse propagation and strong pulse reshaping are expected to occur. These observations will provide stringent tests of the theoretical understanding.

The THz experiments reported here already demonstrate the applicability of TDS for measurements of coherent transients and particularly the recording of the time response of molecules to an external field on a subpicosecond time scale. Additionally, the authors anticipate that an area for future research with great potential is optical pump, THz probe spectroscopy. Time-resolved infrared measurements using a variety of experimental techniques[62−64] have provided a wealth of information on molecular dynamics, but none of these methods are capable of the time resolution in the far-infrared of THz-TDS. To perform a time-resolved THz-TDS study, an optical pump beam would cause photoexcitation, photolysis, or photodissociation of a sample and the resulting rotational distribution would be probed with subpicosecond resolution. Such experiments have been performed with semiconductor samples, but to our knowledge no optical pump THz probe photochemical experiments have yet been done.

It is clear that the capabilities of this relatively young spectroscopic technique have applications for experimental verification of a wide range of problems in physical chemistry and spectroscopy. Continuing improvements in the high-amplitude dynamic range and broad spectral bandwidth of THz spectroscopy will lead to further synergism between experiment and theory, with high-accuracy measurements driving and supporting theoretical development.

Acknowledgment. We acknowledge the key contributions of N. Katzenellenbogen to the work presented here. This work was partially supported by NATO (H.H. and D.G.) under Grant CRG 941172 and by the National Science Foundation (R.A.C. and D.G.) under Grant PHY-9422952.

References and Notes

(1) Townes, C. H.; Schawlow, A. L. *Microwave Spectroscopy*; Dover Publications: New York, 1975.
(2) Fuhr, J. R.; Rozman, L. J.; Wiese, W. L. *NBS Spec. Publ.* **1974**, 366.
(3) Sobelman, I. I.; Vainshtein, L. A.; Yukov, E. A. In *Springer Series: Chemical Physics 7*; Springer-Verlag: Heidelberg, 1981.
(4) Lorentz, H. A. *Proc. Amsterdam Akad. Sci.* **1906**, *8*, 591.
(5) Vleck, J. H. van; Weisskopf, V. F. *Rev. Mod. Phys.* **1945**, *17*, 227.
(6) Frölich, H. *Nature* **1946**, *157*, 478.
(7) Karplus, R.; Schwinger, J. *Phys. Rev.* **1948**, *73*, 1020.
(8) Anderson, P. W. *Phys. Rev.* **1949**, *76*, 647.
(9) Grant, W. B. *Appl. Opt.* **1990**, *29*, 451.
(10) Burch D. E.; Gryvnak, D. A. In *Atmospheric Water Vapor*, Deepak, A., Wilderson, T. D., Ruhnke, L. H., Eds.; Academic Press: New York, 1980.
(11) See, e.g.: Abragam, A. *The Principles of Nuclear Magnetism*: Oxford University Press: New York, 1961.
(12) See, e.g.: Allen, L.; Eberly, J. H. *Optical Resonance and Two-Level-Atoms*; John Wiley & Sons: New York, 1975.
(13) Harde, H.; Keiding, S.; Grischkowsky, D. *Phys. Rev. Lett.* **1991**, *66*, 1834.
(14) Harde, H.; Grischkowsky, D. *J. Opt. Soc. Am. B* **1991**, *8*, 1642.
(15) Harde, H.; Katzenellenbogen, N.; Grischkowsky, D. *J. Opt. Soc. Am. B* **1994**, *11*, 1018.
(16) Harde, H.; Katzenellenbogen, N.; Grischkowsky, D. *Phys. Rev. Lett.* **1995**, *74*, 1307.
(17) Foster, K. L.; Stenholm, S.; Brewer, R. G. *Phys. Rev. A* **1974**, *10*, 2318.
(18) Heritage, J. P.; Gustafson, T. K.; Lin, C. H. *Phys. Rev. Lett.* **1975**, *34*, 1299.
(19) Woerner, M.; Seilmeier, A.; Kaiser, W. *Opt. Lett.* **1989**, *14*, 636.
(20) Bratengeier, K.; Purucker, H. G.; Laubereau, A. *Opt. Commun.* **1989**, *70*, 393.
(21) Robert, D.; Bonamy, J. *J. Phys. (Paris)* **1979**, *40*, 923.
(22) A review with references is given by: Birnbaum, G. In *Advances in Chemical Physics*; J. Wiley: New York, 1967; Vol. 12.
(23) Tsao, C. J.; Curnutte, B. *J. Quant. Spectrosc. Radiat. Transfer* **1962**, *2*, 41.
(24) Boulet, C.; Robert, D.; Galatry, L. *J. Chem. Phys.* **1980**, *72*, 751.
(25) Exter, M. van; Fattinger, Ch.; Grischkowsky, D. *Appl. Phys. Lett.* **1989**, *55*, 337.
(26) Exter, M. van; Fattinger, Ch.; Grischkowsky, D. *Opt. Lett.* **1989**, *14*, 1128.
(27) Exter, M. van; Fattinger, Ch.; Grischkowsky, D. *Laser Spectroscopy IX—Proceedings of the Ninth International Conference on Laser Spectroscopy*; Feld, M. S., Thomas, J. E., Mooradian, A., Eds.; Academic Press: San Diego, CA, 1989.
(28) Grischkowsky, D.; Keiding, S.; Exter, M. van; Fattinger, Ch. *J. Opt. Soc. Am. B* **1990**, *7*, 2006.
(29) Exter, M. van; Grischkowsky, D. *IEEE Trans. Microwave Theory Tech.* **1990**, *38*, 1684.
(30) Katzenellenbogen, N.; Grischkowsky, D. *Appl. Phys. Lett.* **1991**, *58*, 222.
(31) Ralph, S. E.; Grischkowsky, D. *Appl. Phys. Lett.* **1991**, *59*, 1972.
(32) Johnson, C.; Low, F. J.; Davidson, A. W. *Opt. Eng.* **1980**, *19*, 255.
(33) Kronig, R. L. *J. Opt. Soc. Am.* **1926**, *12*, 547. Kramers, H. A. *Atti Congr. Int. Fis.* **1927**, *2*, 545.
(34) Debye, P. *Polar Molecules*; Chemical Catalog Co.: New York, 1929; Chapter V.
(35) Drude, P. *Ann. Phys.* **1890**, *39*, 504.
(36) Rocard, M. Y. *J. Phys. Radium* **1933**, *4*, 247.
(37) Powles, J. G. *Trans. Faraday Soc.* **1948**, *48*, 802.
(38) Chantry, G. W. *Infrared and Millimeter Waves*; Academic Press: New York, 1983; Vol. 8, Chapter 1.
(39) Dubrelle, A.; Boucher, D.; Burie, J.; Demaison, J. *Chem. Phys. Lett.* **1977**, *45*, 559.
(40) Jepsen, P.; Broderson, S.; Guelavili, G. *J. Mol. Spectrosc.* **1981**, *88*, 378.
(41) Robert, D.; Bonamy, J. *J. Phys. (Paris)* **1979**, *40*, 923.
(42) Boulet, C.; Robert, D.; Galatry, L. *J. Chem. Phys.* **1980**, *72*, 751.
(43) Flanders, B. N.; Cheville, R. A.; Grischkowsky, D.; Scherer, N. F. *J. Phys. Chem.* **1996**, *100*, 11824.
(44) Kindt, J. T.; Schmuttenmaer, C. A. *J. Phys. Chem.* **1996**, *100*, 10373.
(45) Pedersen, J. E.; Keiding, S. R. *IEEE J. Quantum Electron.* **1992**, *28*, 2518.
(46) Gebbie, H. A. *Philos. Trans. R. Soc. London A* **1979**, *293*, 413.
(47) Zavody, A. M.; Emery, R. J.; Gebbie, H. A. *Nature* **1979**, *277*, 462.
(48) Dyke, T. R.; Mack, K. M.; Muenter, J. S. *J. Chem Phys.* **1977**, *66*, 498.
(49) Kassner, J. L.; Suck, S. H.; Hagen, D. E.; Hale, B. N.; Plummer, P. L. M.; Schmitt, J. L.; Lund, L. H.; Zalabsky, R. A.; Thurmann R. E. II; Stoddard, L. E.; Chen, T. S.; Miller, R. C.; Yue, P. C. P.; Anderson, R. J.; Daee, M. *Atmospheric Water Vapor*; Academic Press: New York, 1980.
(50) Cheville, R. A.; Grischkowsky, D. *Opt. Lett.* **1995**, *20*, 1646.
(51) Barnard, J. A.; Bradley, F. N. *Flame and Combustion*; Chapman and Hall: London, 1985.
(52) Gerhardt, Ph.; Lottler, S.; Hohmann, K. H. *Chem. Phys. Lett.* **1987**, *137*, 306.
(53) Howard, J. B.; McKinnon, J. T.; Makarovsky, Y.; Lafleur, A. L.; Johnson, M. E. *Nature* **1991**, *352*, 139.
(54) Burnham, D. C.; Chiao, R. Y. *Phys. Rev.* **1969**, *188*, 667.
(55) Crisp, M. D. *Phys. Rev. A* **1970**, *1*, 1604.
(56) Grieneisen, H. P.; Goldhar, J.; Kurnit, N. A.; Javan, A.; Schlossberg, H. R. *Appl. Phys. Lett.* **1972**, *21*, 559.
(57) Hartmann, H. J.; Laubereau, A. *Opt. Commun.* **1983**, *47*, 117.
(58) Rothenberg, J. E.; Grischkowsky, D.; Balant, A. C. *Phys. Rev. Lett.* **1984**, *53*, 552.
(59) Brewer, R. G. *Frontiers in Laser Spectroscopy*; Balian, R., Haroche, S., Liberman, S., Eds.; North-Holland: Amsterdam, 1977; p 341.
(60) Shoemaker, R. L. In *Laser and Coherence Spectroscopy*; Steinfeld, J. I., Ed.; Plenum Press: New York, 1978; p 197.
(61) Rosatzin, M.; Suter, D.; Lange, W.; Mlynek, J. *J. Opt. Soc. Am. B* **1990**, *7*, 1231.
(62) Rogers, S. A.; Leone, S. R. *Appl Spectrosc.* **1993**, *47*, 1430.
(63) Bernath, P. F. *Annu. Rev. Phys. Chem.* **1990**, *41*, 91.
(64) Hirota, E.; Kawaguchi, K. *Annu. Rev. Phys. Chem.* **1985**, *36*, 53.